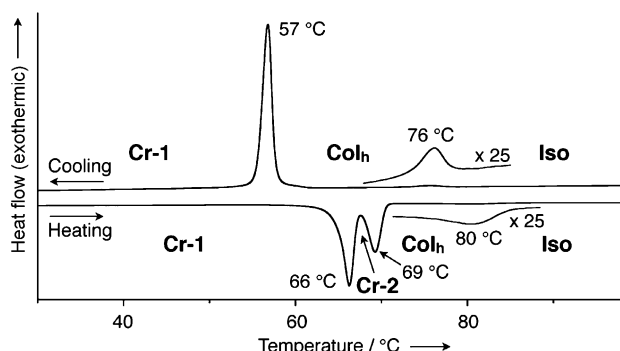




and  $^{13}\text{C}$  NMR spectroscopy and MALDI-TOF mass spectrometry.<sup>[6]</sup>

In differential scanning calorimetry (DSC) studies,  $\mathbf{1}_{\text{TEG}}$  displayed an LC mesophase between 69 and 80 °C (on heating) and between 76 and 57 °C (on cooling; Figure 2;



**Figure 2.** DSC trace for a second heating/cooling cycle (scan rate: 5 °C min<sup>-1</sup>) of  $\mathbf{1}_{\text{TEG}}$ . Cr: crystal, Col<sub>h</sub>: hexagonal columnar LC phase, Iso: isotropic melt.

see also Table S1 in the Supporting Information). The powder X-ray diffraction (XRD) pattern of the LC mesophase of  $\mathbf{1}_{\text{TEG}}$  in a glass capillary showed four peaks with  $d$  spacings of 2.21, 1.27, 1.10, and 0.84 nm (Figure 3a; see also Figure S3 in the Supporting Information), which were indexed as diffractions from the (100), (110), (200), and (210) planes, respectively. Thus, LC  $\mathbf{1}_{\text{TEG}}$  forms a Col<sub>h</sub> structure with a lattice parameter ( $a$ ) of 2.55 nm (Figure 3b, orange hexagon). This value

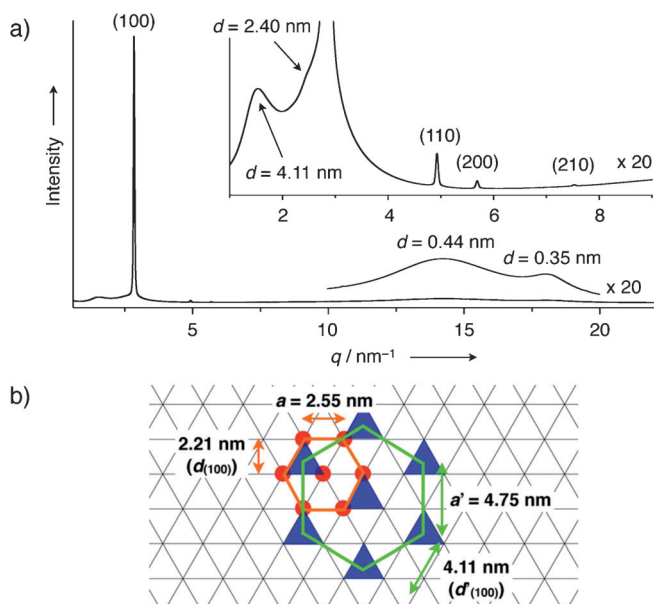


**Figure 3.** a) Synchrotron radiation XRD pattern of  $\mathbf{1}_{\text{TEG}}$  at 75 °C on heating in a glass capillary ( $\phi = 1.5$  mm) and a magnification of the pattern (inset:  $\times 20$ , scattering vector  $q = 1\text{--}9$  nm<sup>-1</sup>). Values in parentheses are Miller indices. b) Schematic illustration of the small (orange) and large (green) hexagonal lattices observed by XRD for LC  $\mathbf{1}_{\text{TEG}}$ .

corresponds to the lateral core-to-core distance between 1D columns of  $\mathbf{1}_{\text{TEG}}$ . The diffraction peak at  $q = 17.8$  nm<sup>-1</sup> can be assigned to the face-to-face distance (0.35 nm) of the  $\pi$ -stacked  $\mathbf{1}_{\text{TEG}}$  molecules along the columnar axis. Two diffraction peaks with  $d$  spacings of 4.11 and 2.40 nm were detected in a smaller-angle region (Figure 3a). By considering the reciprocal spacing ratio (1: $\sqrt{3}$ ), we attributed these peaks to diffractions from the (100) and (110) planes of an additional hexagonal lattice with a lattice parameter ( $a'$ ) of 4.75 nm (Figure 3b, green hexagon). These observations clearly indicate that LC  $\mathbf{1}_{\text{TEG}}$  forms a 2D hexagonal superlattice structure.

As reported previously,<sup>[7]</sup> compound  $\mathbf{1}_{\text{C10}}$ , which bears decyloxy side chains (Figure 1a), forms a Col<sub>h</sub> structure in the LC mesophase with a lattice parameter identical to that of the smaller hexagonal structure observed for LC  $\mathbf{1}_{\text{TEG}}$  (2.55 nm). However, even in a detailed XRD study of  $\mathbf{1}_{\text{C10}}$  with a synchrotron radiation source, we were unable to detect diffraction peaks indicative of the presence of a 2D superlattice (see Figure S5).<sup>[6]</sup> We also investigated the phase behaviors of  $\mathbf{1}_{\text{EG}}$  and  $\mathbf{2}_{\text{TEG}}$  (Figure 1a) by means of DSC and temperature-dependent XRD and found that neither compound exhibited a LC mesophase but rather that both underwent a crystal-to-melt or glass-to-melt transition (see Figures S2, S4, and S6, and Table S1).<sup>[6]</sup> There is a clear difference between the structures of  $\mathbf{1}_{\text{TEG}}$  and  $\mathbf{1}_{\text{C10}}$ , which only bears paraffinic side chains. Compound  $\mathbf{1}_{\text{EG}}$  has oxyethylene side chains, but they are too short to endow the molecule with a distinct amphiphilic character. Although  $\mathbf{2}_{\text{TEG}}$  is similar in structure to  $\mathbf{1}_{\text{TEG}}$ , its benzo[*b*]triphenylene core is devoid of nitrogen atoms, and the existence of a dipole along the longer molecular axis can hardly be expected (see Figure S1b and Table S3).<sup>[6]</sup>

All of the above observations allow us to rationalize the formation of the 2D superlattice structure in LC  $\mathbf{1}_{\text{TEG}}$  as shown in Figure 4. We assume that side-chain miscibility prevails over the dipole–dipole interaction and results in a head-to-head  $\pi$ -stacking arrangement of  $\mathbf{1}_{\text{TEG}}$  (Figure 4b). To minimize both the net dipole of the LC system and the contact area of the immiscible side chains,  $\pi$ -stacked columns of  $\mathbf{1}_{\text{TEG}}$  assemble triangularly into a cylindrical architecture (Figure 4c), with the TEG side chains localized in the center. It is likely that the resultant cylinders, each of which consists of three columns of  $\pi$ -stacked  $\mathbf{1}_{\text{TEG}}$ , arrange laterally to form an extended hexagonal lattice (Figure 4d). Indeed, the small ( $a = 2.55$  nm) and large lattice parameters ( $a' = 4.75$  nm) determined by XRD are consistent with the geometry of the proposed hierarchical structure.

Interestingly, the LC columns of hierarchically assembled  $\mathbf{1}_{\text{TEG}}$  spontaneously align homeotropically on a glass substrate. Under a polarized optical microscope (POM), a film of  $\mathbf{1}_{\text{TEG}}$  sandwiched between glass plates at a mesophase temperature (75 °C) showed a dark field over a large area (Figure 5a, inset). On the other hand, optical microscopy (OM) showed dendritic textures (Figure 5a). These observations are typical for homeotropically aligned Col<sub>h</sub> assemblies.<sup>[8]</sup> In contrast, a POM image of an LC film of paraffinic  $\mathbf{1}_{\text{C10}}$  showed both bright birefringent texture and a dark field as a result of LC domains of horizontally and homeotropically aligned col-

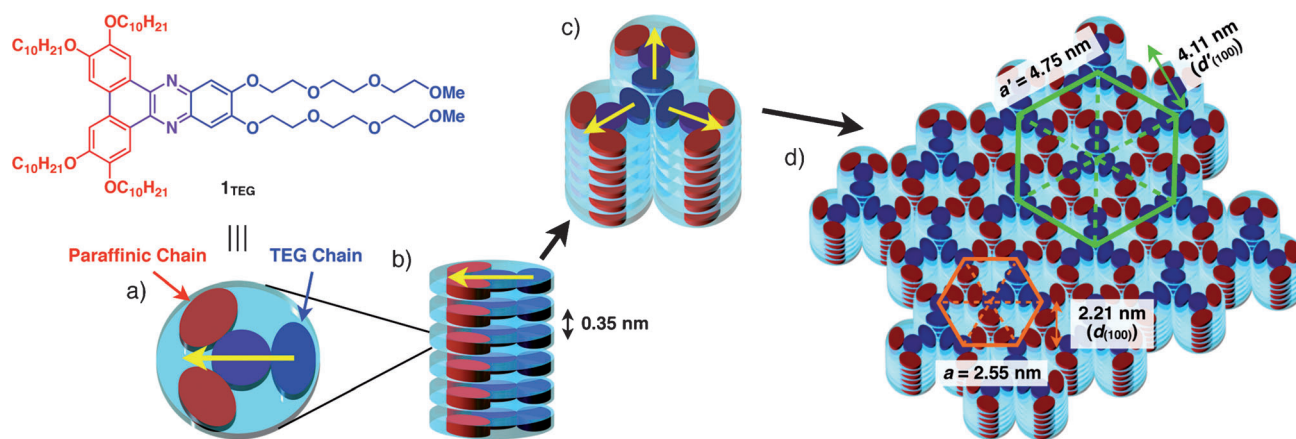


**Figure 4.** Hierarchical self-assembly of  $\mathbf{1}_{\text{TEG}}$ : a)  $\mathbf{1}_{\text{TEG}}$  molecule; b)  $\pi$ -stacked column of  $\mathbf{1}_{\text{TEG}}$  with a head-to-head arrangement; c) triangular assembly of  $\pi$ -stacked columns; d) hexagonal superlattice with structural parameters indicated. The yellow arrows indicate the dipole moment of the dibenzo[*a,c*]phenazine core.

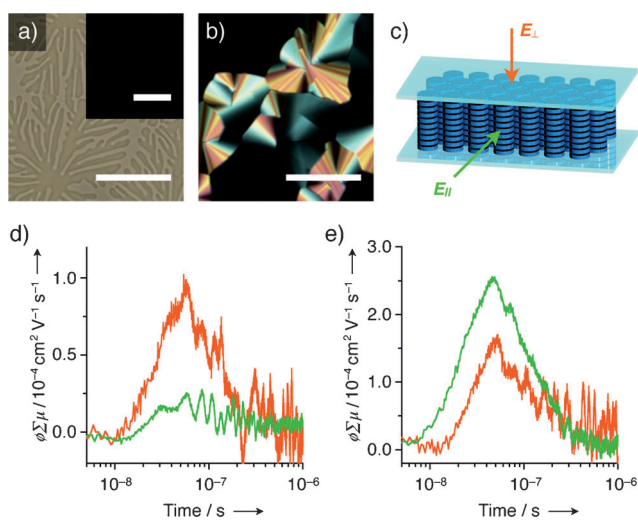


**Figure 5.** a) OM micrograph (inset: POM micrograph) of  $\mathbf{1}_{\text{TEG}}$  at 75 °C and b) POM micrograph of  $\mathbf{1}_{\text{C10}}$  at 100 °C, on cooling from the isotropic melt (scale bar: 50  $\mu\text{m}$ ). c) Schematic illustration of an LC film of  $\mathbf{1}_{\text{TEG}}$  sandwiched between quartz plates for an FP-TRMC experiment. d,e) FP-TRMC profiles at 70 °C of LC films of  $\mathbf{1}_{\text{TEG}}$  (d) and  $\mathbf{1}_{\text{C10}}$  (e) as measured perpendicular (orange) and parallel (green) to the microwave electric-field vector.

mnms, respectively (Figure 5b). Thus, LC  $\mathbf{1}_{\text{C10}}$  does not adopt a homeotropic orientation predominantly.

The contrasting orientational behavior of LC  $\mathbf{1}_{\text{TEG}}$  and  $\mathbf{1}_{\text{C10}}$  was clearly demonstrated by the measurement of flash-photolysis time-resolved microwave conductivity (FP-TRMC). The FP-TRMC technique enables the evaluation, without electrodes, of the intrinsic carrier-transport properties of materials.<sup>[9]</sup> For this experiment, an LC film of  $\mathbf{1}_{\text{TEG}}$  sandwiched between two quartz plates was placed in a microwave resonant cavity in such a way that the microwave electric-field (*E*-field) vector could be polarized either perpendicular or parallel to the substrate surface (Figure 5c). Upon exposure of the LC film to laser light, the transient conductivity of the LC film displayed a rise and decay profile, whereby the transient conductivity is given by  $\phi\Sigma\mu$ , and  $\phi$  and

$\Sigma\mu$  are the photocarrier-generation yield and the sum of the mobilities of generated charge carriers, respectively (Figure 5d). From the FP-TRMC profile, the maximum transient conductivities ( $\phi\Sigma\mu_{\text{max}}$ ) along the perpendicular (orange) and parallel (green) directions to the substrate surface were evaluated as  $1.0 \times 10^{-4}$  and  $2.7 \times 10^{-5} \text{ cm}^2 \text{ V}^{-1} \text{ s}^{-1}$ , respectively. Accordingly, the degree of anisotropy ( $\phi\Sigma\mu_{\perp} / \phi\Sigma\mu_{\parallel}$ ) in the LC film of  $\mathbf{1}_{\text{TEG}}$  was calculated to be 3.7. Although an LC film of  $\mathbf{1}_{\text{C10}}$  also displayed a FP-TRMC signal (Figure 5e), the value of  $\phi\Sigma\mu_{\perp}$  ( $1.7 \times 10^{-4} \text{ cm}^2 \text{ V}^{-1} \text{ s}^{-1}$ ) was lower than that of  $\phi\Sigma\mu_{\parallel}$  ( $2.6 \times 10^{-4} \text{ cm}^2 \text{ V}^{-1} \text{ s}^{-1}$ ), and the degree of anisotropy was as small as 0.7.

It has been suggested that the homeotropic columnar orientation of LC materials is possible when nucleation occurs from a glass/LC interface rather than from the bulk.<sup>[10]</sup> A recent report also showed that long-range 2D lattice order can be a dominant factor for such a columnar orientation.<sup>[11]</sup> In light of these notions, the strong preference of LC  $\mathbf{1}_{\text{TEG}}$  for a homeotropic orientation most likely results from the hierarchical superlattice structure, which could enhance the 2D order of columnar assembly of  $\mathbf{1}_{\text{TEG}}$  to a certain upper length scale. Furthermore, the TEG side chains of  $\mathbf{1}_{\text{TEG}}$  localize at each lattice point of the superlattice (Figure 4d), and this arrangement gives rise to hydrophilic domains that can potentially interact with hydroxy groups on a  $\text{SiO}_2$  substrate. Presumably, such a surface event also plays a role in the development of homeotropic alignment.

In conclusion, we demonstrated that the LC dibenzo[*a,c*]phenazine  $\mathbf{1}_{\text{TEG}}$ , which contains decyloxy and TEG side chains, self-assembles to form a 2D hexagonal superlattice. This type of hierarchical structure has not previously been reported for columnar LC assemblies composed of disk-shaped aromatic molecules. In contrast to most reported examples,<sup>[12]</sup> we ventured to adopt a molecular design that could hamper a head-to-tail packing arrangement, which is favorable for the canceling out of dipoles between adjacent molecules. As a consequence,  $\mathbf{1}_{\text{TEG}}$  chooses an unprecedented way to cancel out the dipoles in the LC material: 1D triangular assemblies consisting of three  $\pi$ -stacked columns of  $\mathbf{1}_{\text{TEG}}$  arrange laterally to form a large hexagonal lattice

(Figure 4). Interestingly, the hierarchically assembled LC columns of  $\mathbf{1}_{\text{TEG}}$  tend to align homeotropically on a glass substrate over a large area and could thus provide pathways for directional charge transport perpendicular to the substrate.

Received: September 24, 2012

Published online: November 26, 2012

**Keywords:** amphiphiles · dipole–dipole interactions · liquid crystals · organic semiconductors · self-assembly

- [1] a) F. J. M. Hoeben, P. Jonkheijm, E. W. Meijer, A. P. H. J. Schenning, *Chem. Rev.* **2005**, *105*, 1491–1546; b) J. Wu, W. Pisula, K. Müllen, *Chem. Rev.* **2007**, *107*, 718–747; c) S. Laschat, A. Baro, N. Steinke, F. Giesselmann, C. Hägele, G. Scalia, R. Judele, E. Kapatsina, S. Sauer, A. Schreivogel, M. Tosoni, *Angew. Chem.* **2007**, *119*, 4916–4973; *Angew. Chem. Int. Ed.* **2007**, *46*, 4832–4887; d) M. O'Neill, S. M. Kelly, *Adv. Mater.* **2011**, *23*, 566–584.
- [2] a) M. Yoshio, T. Mukai, H. Ohno, T. Kato, *J. Am. Chem. Soc.* **2004**, *126*, 994–995; b) K. Binnemans, *Chem. Rev.* **2005**, *105*, 4148–4204; c) H. Shimura, M. Yoshio, K. Hoshino, T. Mukai, H. Ohno, T. Kato, *J. Am. Chem. Soc.* **2008**, *130*, 1759–1765.
- [3] a) H. Bengs, M. Ebert, O. Karthaus, B. Kohne, K. Praefcke, H. Ringsdorf, J. H. Wendroff, R. Wüstefeld, *Adv. Mater.* **1990**, *2*, 141–144; b) N. Boden, R. J. Bushby, J. Clements, *J. Chem. Phys.* **1993**, *98*, 5920–5931; c) A. Okabe, T. Fukushima, K. Ariga, T. Aida, *Angew. Chem.* **2002**, *114*, 3564–3567; *Angew. Chem. Int. Ed.* **2002**, *41*, 3414–3417.
- [4] a) E. J. Foster, C. Lavigneur, Y.-C. Ke, V. E. Williams, *J. Mater. Chem.* **2005**, *15*, 4062–4068; b) E. J. Foster, R. B. Jones, C. Lavigneur, V. E. Williams, *J. Am. Chem. Soc.* **2006**, *128*, 8569–8574; c) C. Lavigneur, E. J. Foster, V. E. Williams, *J. Am. Chem. Soc.* **2008**, *130*, 11791–11800; d) E. Voisin, E. J. Foster, M. Rakotomalala, V. E. Williams, *Chem. Mater.* **2009**, *21*, 3251–3261; e) J. A. Paquette, C. J. Yardley, K. M. Psutka, M. A. Cochran, O. Calderon, V. E. Williams, K. E. Maly, *Chem. Commun.* **2012**, *48*, 8210–8212.
- [5] a) C. A. Hunter, J. K. M. Sanders, *J. Am. Chem. Soc.* **1990**, *112*, 5525–5534; b) F. Cozzi, M. Cinquini, R. Annunziata, T. Dwyer, J. S. Siegel, *J. Am. Chem. Soc.* **1992**, *114*, 5729–5733; c) F. Cozzi, M. Cinquini, R. Annunziata, J. S. Siegel, *J. Am. Chem. Soc.* **1993**, *115*, 5330–5331; d) F. Cozzi, F. Ponzini, R. Annunziata, M. Cinquini, J. S. Siegel, *Angew. Chem.* **1995**, *107*, 1092–1094; *Angew. Chem. Int. Ed. Engl.* **1995**, *34*, 1019–1020.
- [6] See the Supporting Information.
- [7] C. W. Ong, J.-Y. Hwang, M.-C. Tzeng, S.-C. Liao, H.-F. Hsu, T.-H. Chang, *J. Mater. Chem.* **2007**, *17*, 1785–1790.
- [8] I. Dierking, *Textures of Liquid Crystals*, Wiley-VCH, Weinheim, **2003**, chap. 11, pp. 145–153.
- [9] A. Saeki, S. Seki, T. Takenobu, Y. Iwasa, S. Tagawa, *Adv. Mater.* **2008**, *20*, 920–923.
- [10] E. Grelet, H. Bock, *Europhys. Lett.* **2006**, *73*, 712–718.
- [11] T. Osawa, T. Kajitani, D. Hashizume, H. Ohsumi, S. Sasaki, M. Takata, Y. Koizumi, A. Saeki, S. Seki, T. Fukushima, T. Aida, *Angew. Chem.* **2012**, *124*, 8114–8117; *Angew. Chem. Int. Ed.* **2012**, *51*, 7990–7993.
- [12] a) J. A. Rego, S. Kumar, H. Ringsdorf, *Chem. Mater.* **1996**, *8*, 1402–1409; b) S. T. Trzaska, T. M. Swager, *Chem. Mater.* **1998**, *10*, 438–443; c) K. Kishikawa, S. Furusawa, T. Yamaki, S. Kohmoto, M. Yamamoto, K. Yamaguchi, *J. Am. Chem. Soc.* **2002**, *124*, 1597–1605; d) R. J. Bushby, N. Boden, C. A. Kilner, O. R. Lozman, Z. Lu, Q. Liu, M. A. Thornton-Pett, *J. Mater. Chem.* **2003**, *13*, 470–474; e) S. J. Mahoney, M. M. Ahmida, H. Kayal, N. Fox, Y. Shimizu, S. H. Eichhorn, *J. Mater. Chem.* **2009**, *19*, 9221–9232; f) H.-C. Chang, K. Komasa, K. Kishida, T. Shiozaki, T. Ohmori, T. Matsumoto, A. Kobayashi, M. Kato, S. Kitagawa, *Inorg. Chem.* **2011**, *50*, 4279–4288.